

Stagnation of subducting slabs in the transition zone due to slow diffusion in majoritic garnet

W. L. van Mierlo^{1*}†, F. Langenhorst^{1,2}, D. J. Frost¹ and D. C. Rubie¹

Oceanic lithosphere sinks into Earth's mantle at subduction zones. However, seismic tomography shows that the sinking slabs of lithosphere often stagnate in the lower part of the mantle transition zone¹, at depths less than 660 km, where rocks undergo pressure-induced phase transitions and become denser. Greater pressures are required to induce phase transitions in cold slabs compared with the hotter ambient mantle at the 660 km discontinuity, and so, at the boundary between the transition zone and the lower mantle, the slabs are buoyant². The slabs may also contain low-density minerals that could contribute to their buoyancy³. Here we use laboratory experiments to analyse the rate of dissolution of the common slab mineral pyroxene into garnet, at pressures and temperatures representative of the lower part of the mantle transition zone. We find that the majorite component in garnet—a product of the transition from pyroxene into garnet—is one of the slowest-diffusing components in Earth's mantle. **At the relatively low temperatures of the slab, this slow diffusion inhibits the dissolution of pyroxene into garnet, so that the slab remains buoyant relative to the ambient mantle and stagnates. However, at the base of the mantle transition zone, pyroxene undergoes another phase transformation to the mineral akimotoite, which causes a sudden increase in slab density. We conclude that the slab is likely to penetrate into the lower mantle eventually.**

In the upper mantle, garnets are dominated by the pyrope endmember (that is, $Mg_3Al_2Si_3O_{12}$). However, at conditions of Earth's mantle transition zone (410–660 km depth) garnets should contain large proportions of the majorite component, which has the stoichiometry of pyroxene (that is, $Mg_4Si_4O_{12}$), and arises from the coupled substitution of Mg and Si into the octahedrally coordinated Al site in garnet. Under equilibrium conditions majoritic garnet makes up 40–60 volume% of Earth's transition zone^{4,5}, whereas subducted oceanic crust under the same conditions would consist of up to 80 volume % majoritic garnet⁶. Mantle garnets become progressively majoritic at pressures above 6 GPa at the expense of ortho and clinopyroxene, with the result that the transition zone is considered to be free of pyroxene at pressures above ~18 GPa (refs 5–7). Thus, under equilibrium conditions, the pyroxene to garnet reaction occurs over a wide pressure range. However, the kinetics of this reaction must be controlled by the rate of diffusion of the majorite component in garnet. So far only qualitative reports have been published through which to assess this diffusion rate^{8,9}.

We performed diffusion experiments on **majorite–natural pyrope diffusion couples** in a multianvil apparatus at mantle transition zone conditions. The submicrometre diffusion profiles

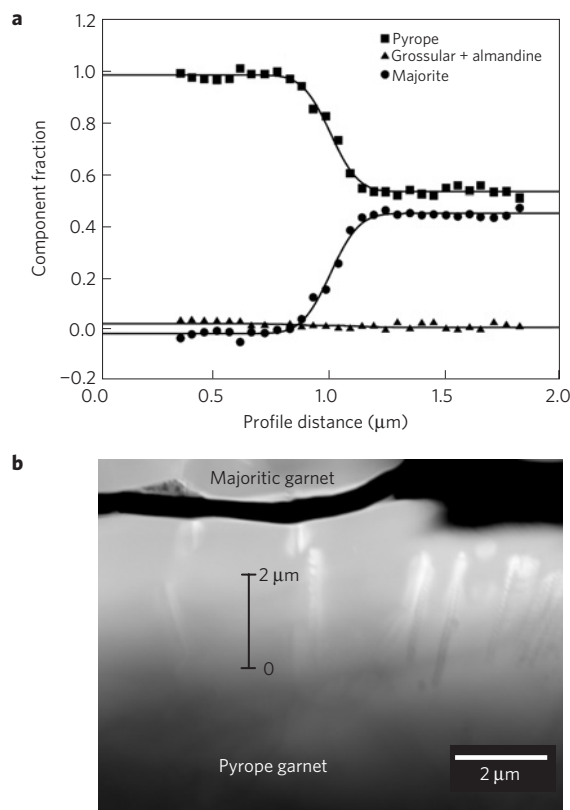


Figure 1 | Diffusion profiles obtained from a pyrope–majorite diffusion couple H3050. a, The concentration profiles expressed in garnet endmember fractions. The negligible almandine and grossular components have been summed up as one virtual component. The symbols denote quantitative EDX–TEM data and the lines show fitted diffusion profiles. **b**, The location (solid black line) of the diffusion profile in **a**. The original boundary between the diffusion couple halves migrated into the majoritic garnet and is at the position of the black crack near the top of the figure. See Supplementary Notes for a more detailed discussion.

were measured by transmission electron microscopy (TEM) and subsequently compositionally independent diffusion coefficients for each component were fitted to the profiles (see Methods). Typical diffusion profiles, expressed in terms of the conventional garnet components, are shown in Fig. 1 for a pyrope–majorite experiment performed at 1,800 °C for 2 h. From the profiles, the

¹Bayerisches Geoinstitut, Universität Bayreuth, D-95440 Bayreuth, Germany, ²Institut für Geowissenschaften, Friedrich-Schiller-Universität Jena, Carl-Zeiss-Promenade 10, D-07745 Jena, Germany. †Present address: Materialwissenschaftliche Elektronenmikroskopie, Universität Ulm, Albert-Einstein-Allee 11, D-89081 Ulm, Germany. *e-mail: willem.van-mierlo@uni-ulm.de.

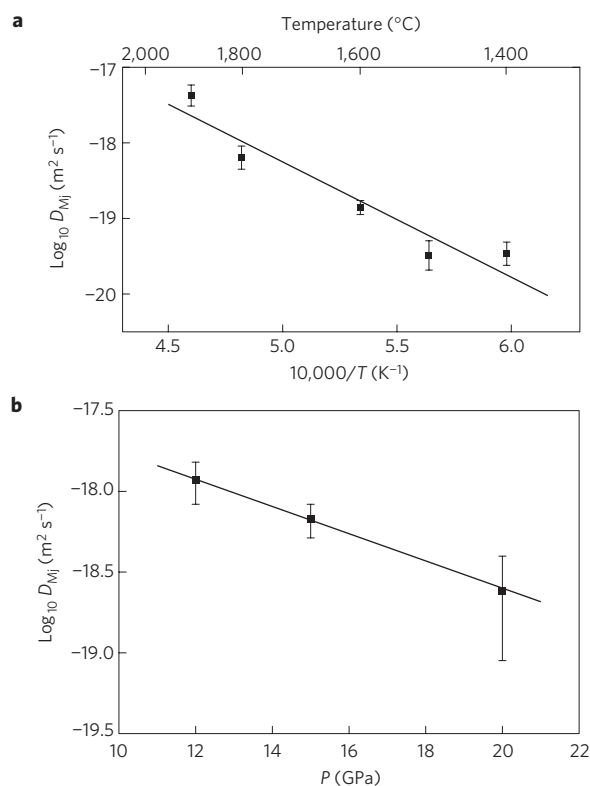


Figure 2 | Diffusion coefficients for majorite diffusion in garnet as a function of temperature and pressure. **a**, Results of diffusion experiments performed between 1,400 and 1,900 °C at 15 GPa. **b**, Results of diffusion experiments performed between 12 and 20 GPa at 1,800 °C. Error bars indicate uncertainties obtained from the fitting of the diffusion coefficients to the measured profiles at the 90% confidence interval.

effective binary diffusion coefficients¹⁰ for the pyrope and majorite components were determined to be $D_{Py} = 6(2) \times 10^{-19} \text{ m}^2 \text{ s}^{-1}$ and $D_{Mj} = 7(1) \times 10^{-19} \text{ m}^2 \text{ s}^{-1}$, respectively.

Garnet diffusion coefficients determined from pyrope–majorite experiments at 15 GPa are shown in Fig. 2a as a function of inverse temperature. The activation enthalpy for diffusion of the majorite component in garnet, obtained by fitting the measured binary diffusion coefficient to an Arrhenius equation, is $291 \pm 51 \text{ kJ mol}^{-1}$ with the pre-exponential factor being $2.3 \times 10^{-11} \text{ m}^2 \text{ s}^{-1}$ (the confidence interval lies between the two limiting values 9.4×10^{-14} and $5.4 \times 10^{-10} \text{ m}^2 \text{ s}^{-1}$, all reported errors are at the 68% confidence level unless stated otherwise). For the pyrope component the values are within error the same. The effect of pressure on the diffusivity was determined from experiments performed at 1,800 °C and 12, 15 and 20 GPa, using the same pyrope–majorite garnet diffusion couples as in the experiments described above. The results of the three

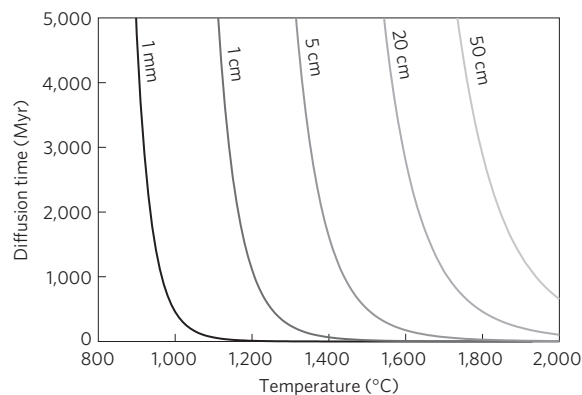


Figure 3 | Diffusion distance for the majorite component in garnet at 18 GPa. The diffusion distance has been calculated as a function of diffusion time and temperature. The main mechanism of mass transport is assumed to be volume diffusion.

diffusion experiments are shown in Fig. 2b and listed in Table 1. The diffusivity of the majorite component in garnet decreases from $1.2(2) \times 10^{-18} \text{ m}^2 \text{ s}^{-1}$ at 12 GPa to $2.4(8) \times 10^{-19} \text{ m}^2 \text{ s}^{-1}$ at 20 GPa and the resulting activation volume for diffusion of the majorite component in garnet was determined to be $3.3(1) \text{ cm}^3 \text{ mol}^{-1}$. Combining this with the previously determined activation enthalpy at 15 GPa, we derive an activation energy for diffusion of the majorite component in garnet of $241 \pm 54 \text{ kJ mol}^{-1}$ and a pre-exponential factor of $1.4 \times 10^{-11} \text{ m}^2 \text{ s}^{-1}$ (the confidence interval lies between the two limiting values 5.6×10^{-13} and $3.5 \times 10^{-10} \text{ m}^2 \text{ s}^{-1}$).

Wadsleyite and ringwoodite are the most abundant mineral phases that coexist with majoritic garnet in the mantle transition zone. A comparison of the results of this study with other diffusion studies shows that at 1,500 °C diffusion of the majorite component in garnet is about 7 orders of magnitude slower than Fe–Mg interdiffusion in wadsleyite at 15 GPa (refs 11,12) and similar to the rates of silicon diffusion in wadsleyite and ringwoodite at the conditions at which these phases are stable^{12,13}. Extrapolation of the data to pressures of the top of the lower mantle shows that at 1,700 °C diffusion of the majorite component in garnet is even slower than both the diffusion of silicon and Fe–Mg interdiffusion in silicate perovskite (at an oxygen fugacity near or above the iron–wüstite buffer)¹⁴. It is, therefore, one of the slowest-diffusing chemical components in Earth’s mantle.

Our diffusion data can be used to estimate equilibration times and distances over which chemical heterogeneities, characterized by lithologies with different garnet compositions and proportions, can be homogenized in Earth’s transition zone. Through the subduction of oceanic lithosphere, large-scale chemical heterogeneities are introduced into the mantle at rates of several centimetres per year but in many instances subducting slabs stagnate at the base of the transition zone². The major mantle lithologies in the transition

Table 1 | Run conditions of the experiments.

Run number	Pressure	Temperature	Run duration	$D_{Py} \text{ (m}^2 \text{ s}^{-1}\text{)}$	$D_{Mj} \text{ (m}^2 \text{ s}^{-1}\text{)}$
H3257	15 GPa	1,400 °C	24 h	$2.5(8) \times 10^{-20}$	$3.4(8) \times 10^{-20}$
H3076	15 GPa	1,500 °C	24 h	$4(2) \times 10^{-20}$	$3(1) \times 10^{-20}$
H2986	15 GPa	1,600 °C	4 h	$1.4(2) \times 10^{-19}$	$1.4(2) \times 10^{-19}$
H3050	15 GPa	1,800 °C	2 h	$6(2) \times 10^{-19}$	$7(1) \times 10^{-19}$
H3106	15 GPa	1,900 °C	2 h	$3.7(7) \times 10^{-18}$	$4(1) \times 10^{-18}$
H3084	20 GPa	1,800 °C	20 h	$2.2(7) \times 10^{-19}$	$2(1) \times 10^{-19}$
H3201	12 GPa	1,800 °C	4 h	$9(5) \times 10^{-19}$	$1.2(3) \times 10^{-18}$

Reported errors are at the 90% confidence level.

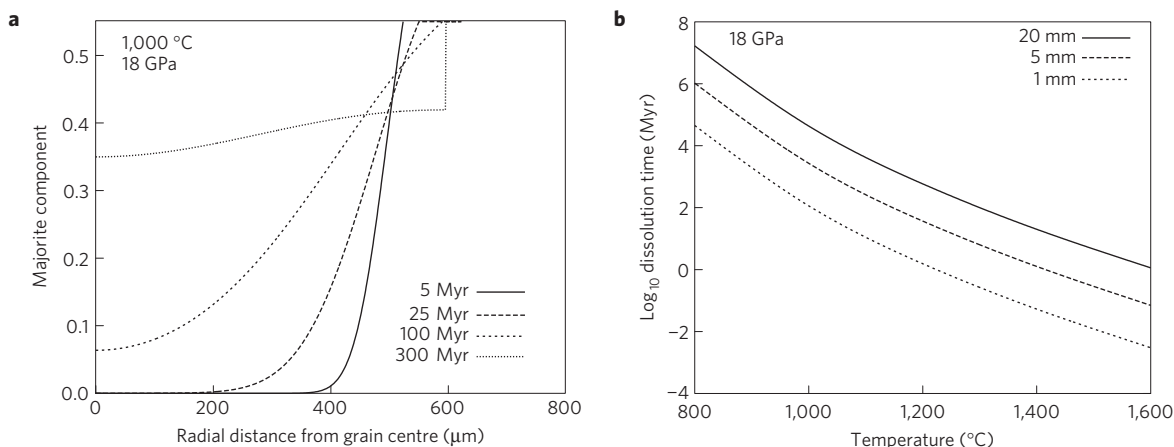


Figure 4 | Timescales for the dissolution of pyroxene into garnet during subduction. **a**, Concentration profiles at different times for diffusion-controlled growth of a spherical garnet grain surrounded by pyroxene that acts as the majorite source. Initial grain diameter is 1 mm; final grain diameter is 1.18 mm. After ~100 Myr all pyroxene is dissolved into garnet, with homogenization after 300 Myr. **b**, Dissolution timescales for different grain sizes representative of the bulk mantle. The exact dependence on temperature is nonlinear because the equilibrium garnet composition at the interface also depends on temperature. The composition of the interface was taken from the literature^{23,29}.

zone, that is, subducted oceanic crust, subducted suboceanic mantle and fertile mantle peridotite, have chemical differences that are expressed mainly in terms of differences in the contents and composition of majoritic garnet. A fundamental question concerns the spatial extent over which solid-state diffusion of the majorite component can homogenize such large-scale heterogeneities, or more realistically, the length scale to which such heterogeneities would have to be stretched or thinned by mantle convection before chemical homogenization could occur in the transition zone. To answer this question, we calculated the distance that the majorite component can diffuse as a function of temperature and time. Volume diffusion was chosen as the main mode of mass transport. The length scale of heterogeneities that can be homogenized can be approximated by $x = 2\sqrt{(D_{\text{vol}} \times t)}$, where D_{vol} is the volume diffusion coefficient and t is the diffusion time, after equation 4.17 and Fig. 4.1 in ref. 15. The temperatures for the ambient transition zone, that is, far away from any subducting slab, have been estimated from thermal models of the mantle^{16–18}, and span 1,450 to 1,800 °C, depending on the exact depth and the distance from subduction zones. Figure 3 shows that the maximum distance the majorite component is able to diffuse in the transition zone is 5–50 cm over a timescale of the age of the Earth. The temperatures in the cold interior of a subducted slab are commonly assumed to be well below 1,000 °C. At such low temperatures diffusion is possible only over distances of less than a millimetre. Although the mantle is polycrystalline, grain boundary diffusion is not expected to enhance the diffusion distance by more than a factor 50 for reasonable transition zone grain size estimates and grain boundary diffusivities (see Supplementary Notes). Solid-state diffusion cannot, therefore, homogenize subducted oceanic crust over more than 25 m within the bulk of the mantle. Hence, subducted lithospheric material will persist as chemical heterogeneities in the convecting mantle throughout the evolution of the Earth, unless intense deformation and/or fluid influx strongly catalyses the rate of equilibration reactions.

Majoritic garnet can crystallize within a few hours in high-pressure phase equilibrium experiments that are performed on glass or fine-grained (for example <2 μm) crushed powdered starting materials at relatively high temperatures¹⁹. Owing to the highly reactive nature of the starting materials, such experiments do not provide information about kinetics in Earth's mantle where rocks are well sintered with grain sizes of the order of millimetres²⁰. However, our new diffusion data can be used to assess the extent

to which chemical equilibrium is maintained between crystals of garnet and pyroxene as they react in the various lithologies of subducting slabs. To model the effect of diffusion on the kinetics of the pyroxene to garnet reaction, we have modelled spherically symmetric diffusion of the enstatite component into a spherical grain of initially pure pyrope combined with the diffusion-controlled growth of this grain (see Supplementary Methods).

First we consider the case for the oceanic crust component of subducting lithosphere. The initial grain size is taken as 1 mm, which is a typical minimum grain size for eclogites²¹. Representative pressure–temperature conditions for the oceanic crust in the transition zone are taken to be 1,000 °C and 18 GPa (ref. 22). The composition of the rim of the garnet grain was fixed at $\text{Py}_{45}\text{Mj}_{55}$, which is the equilibrium composition at the above conditions²³. As the bulk system is undersaturated in pyroxene⁶, a maximum influx of majorite was chosen such that the final garnet composition after complete equilibration is $\text{Py}_{60}\text{Mj}_{40}$, after which dissolution of pyroxene into garnet is stopped. The resulting concentration profiles in the spherical garnet grain after four different times at 1,000 °C and 18 GPa are shown in Fig. 4. The results show that it takes ~100 Myr to fully dissolve the pyroxene component into the garnet. The subducting slab needs about 10–15 Myr to pass through the transition zone, assuming an average subduction rate of 20 mm yr⁻¹. After 12.5 Myr only about 35% of the pyroxene has dissolved into garnet. It is thus unlikely that subducted oceanic crust can reach a state of thermodynamic equilibrium and a metastable mineral assemblage consisting of pyroxene and pyrope-rich garnet is thus expected to be present in subducted oceanic crust. To reach thermodynamic equilibrium the oceanic crust needs to heat up, which requires that the slab remains for a prolonged period in the transition zone.

Second we consider the case for subducting peridotitic mantle, which would experience temperatures that range from below that of the oceanic crust (<1,000 °C), up to the ambient mantle temperature (1,600 °C; refs 22,24). Peridotites typically have grain sizes larger than 1 mm (ref. 25). Dissolution timescales for grain sizes from 1 to 20 mm are plotted in Fig. 4b. This shows that dissolution of pyroxene into garnet would take several billion years at 1,000 °C. Only when the temperature of the subducted slab has increased to at least 1,400 °C would chemical equilibration occur on a geologically reasonable timescale of a few million years. Therefore, most of the subducted lithospheric mantle is also not expected to thermodynamically equilibrate during

subduction and will transport metastable mineral assemblages into the transition zone.

The metastable persistence of pyroxene in both the oceanic crust and peridotitic components of a subducting slab has two important implications for mantle dynamics. First, the density of the down-going slab will initially remain low during subduction (we estimate a 1–2% reduction in density), contributing to slab deceleration and possibly transient stagnation in the transition zone. Second, as the slab enters the deeper transition zone, it is likely that metastable pyroxene will undergo phase transformations directly to higher-pressure polymorphs²⁶, resulting, in turn, in a large density increase. Subducted lithospheric mantle, particularly the harzburgitic layer, contains up to 40 vol% enstatitic pyroxene that could transform directly into metastable akimotoite when the pressure reaches ~19 GPa (ref. 26), corresponding to a depth of 550 km, with a huge density increase of ~16%. The existence of such metastable akimotoite-bearing slab regions in the Tonga slab has recently been proposed on the basis of seismic anisotropy²⁷. Such a large increase in density would cause the remobilization of a stagnant slab and catalyse its descent into the lower mantle. Thus, slab dynamics in the mantle transition zone are likely to be controlled to a large extent by metastability and the kinetics of pyroxene-breakdown reactions.

Methods

Diffusion experiments with polycrystalline majoritic garnet–natural pyrope diffusion couples have been conducted in a 1,200 ton multianvil apparatus between 1,400 °C and 1,900 °C and from 12 GPa to 20 GPa. After recovery, the samples were prepared for TEM investigation by mechanical polishing followed either by argon-milling or focused ion beam preparation. The diffusion profiles have been measured in scanning transmission electron microscope mode using a Philips CM20 TEM at 200 kV equipped with an energy-dispersive X-ray (EDX) detector. To obtain the diffusion coefficients from the measured profiles, the profiles have been fitted by a numerical finite-difference model with a constant (that is, compositionally independent) diffusion coefficient for each component. Note that rather than characterizing diffusion in terms of individual elements²⁸, we can describe diffusion in terms of garnet components because the diffusion of the individual elements (for example, Mg and Si) must be coupled to preserve charge balance. Furthermore, within error, the diffusion coefficients for both the components in the majorite–pyrope diffusion experiments are identical. This is to be expected because the concentrations of the grossular and almandine components are very low such that the experiments basically involve binary diffusion between the pyrope and majorite components, which can be characterized by a single diffusion coefficient.

In the Supplementary Information a more detailed description of the experimental, analytical and computational methods used in this study is given.

Received 4 October 2012; accepted 14 February 2013;
published online 31 March 2013

References

- Káráson, H. & Van der Hilst, R. D. in *The History and Dynamics of Global Plate Motion* Vol. 121 (eds Richards, M. R., Gordon, R. & Van der Hilst, R. D.) 277–288 (American Geophysical Union, 2000).
- Fukao, Y., Obayashi, M. & Nakakuki, T. Stagnant slab: A review. *Annu. Rev. Earth Planet. Sci.* **37**, 19–46 (2009).
- Tetzlaff, M. & Schmelting, H. The influence of olivine metastability on deep subduction of oceanic lithosphere. *Phys. Earth. Planet. Inter.* **120**, 29–38 (2000).
- Bass, J. D. & Parise, J. B. Deep earth and recent developments in mineral physics. *Elements* **4**, 157–165 (2008).
- Frost, D. J. The upper mantle and transition zone. *Elements* **4**, 171–176 (2008).
- Irifune, T., Sekine, T., Ringwood, A. E. & Hibberson, W. O. The eclogite–garnetite transformation at high pressure and some geophysical implications. *Earth. Planet. Sci. Lett.* **77**, 245–256 (1986).
- Ganguly, J., Freed, A. M. & Saxena, S. K. Density profiles of oceanic slabs and surrounding mantle: Integrated thermodynamic and thermal modelling, and implications for the fate of slabs at the 660 km discontinuity. *Phys. Earth. Planet. Inter.* **172**, 257–267 (2009).
- Nishi, M., Kato, T., Kubo, T. & Kikegawa, T. Survival of pyropic garnet in subducting plates. *Phys. Earth. Planet. Inter.* **170**, 274–280 (2008).
- Nishi, M., Kubo, T. & Kato, T. Metastable transformations of eclogite to garnetite in subducting oceanic crust. *J. Mineral. Petrol. Sci.* **104**, 192–198 (2009).
- Chakraborty, S. & Ganguly, J. Cation diffusion in aluminosilicate garnets: Experimental determination in spessartine–almandine diffusion couples, evaluation of effective binary diffusion coefficients, and applications. *Contrib. Mineral. Petrol.* **111**, 74–86 (1992).
- Holzappel, C., Chakraborty, S., Rubie, D. C. & Frost, D. J. Fe–Mg interdiffusion in wadsleyite: The role of pressure, temperature and composition and the magnitude of jump in diffusion rates at the 410 km discontinuity. *Phys. Earth. Planet. Inter.* **172**, 28–33 (2009).
- Chakraborty, S. Diffusion coefficients in olivine, wadsleyite and ringwoodite. *Rev. Mineral. Geoch.* **72**, 603–639 (2010).
- Shimojuku, A. et al. Si and O diffusion in (Mg, Fe)₂SiO₄ wadsleyite and ringwoodite and its implications for the rheology of the mantle transition zone. *Earth. Planet. Sci. Lett.* **284**, 103–112 (2009).
- Holzappel, C., Rubie, D. C., Frost, D. J. & Langenhorst, F. Fe–Mg interdiffusion in (Mg, Fe)SiO₃ perovskite and lower mantle reequilibration. *Science* **309**, 1707–1710 (2005).
- Crank, J. *The Mathematics of Diffusion* (Oxford Univ. Press, 1980).
- McKenzie, D. & Bickle, M. J. The volume and composition of melt generated by extension of the lithosphere. *J. Petrol.* **29**, 625–679 (1988).
- Anderson, D. L. The thermal state of the upper mantle; No role for mantle plumes. *Geophys. Res. Lett.* **27**, 3623–3626 (2000).
- Katsura, T., Yoneda, A., Yamazaki, D., Yoshino, T. & Ito, E. Adiabatic temperature profile in the mantle. *Phys. Earth. Planet. Inter.* **183**, 212–218 (2010).
- Akaogi, M. & Akimoto, S. High-pressure phase equilibria in a garnet lherzolite, with special reference to Mg²⁺–Fe²⁺ partitioning among constituent minerals. *Phys. Earth Planet. Inter.* **19**, 31–51 (1979).
- Rubie, D. C. & Thompson, A. B. in *Metamorphic Reactions: Kinetics, Textures and Deformation* Vol. 4 (eds Thompson, A. B. & Rubie, D. C.) 27–79 (Springer, 1985).
- Robinson, P. et al. *Tectono-stratigraphic Setting, Structure and Petrology of HP and UHP Metamorphic Rocks and Garnet Peridotites in the Western Gneiss Region, More and Romsdal, Norway* 142 (NGU, 2003).
- Emmerson, B. & McKenzie, D. Thermal structure and seismicity of subducting lithosphere. *Phys. Earth. Planet. Inter.* **163**, 191–208 (2007).
- Akaogi, M. & Akimoto, S. Pyroxene–garnet solid–solution equilibria in the systems Mg₃Si₄O₁₂–Mg₃Al₂Si₃O₁₂ and Fe₄Si₄O₁₂–Fe₃Al₂Si₃O₁₂ at high pressures and temperatures. *Phys. Earth. Planet. Inter.* **15**, 90–106 (1977).
- Turcotte, D. L. & Schubert, G. *Geodynamics* (Cambridge Univ. Press, 2002).
- Song, S., Zhang, L. & Niu, Y. Ultra-deep origin of garnet peridotite from the North Qaidam ultrahigh-pressure belt, Northern Tibetan Plateau, NW China. *Am. Mineral.* **89**, 1330–1336 (2004).
- Hogrefe, A., Rubie, D. C., Sharp, T. G. & Seifert, F. Metastability of enstatite in deep subducting lithosphere. *Nature* **372**, 351–353 (1994).
- Shiraishi, R., Ohtani, E., Kanagawa, K., Shimojuku, A. & Zhao, D. Crystallographic preferred orientation of akimotoite and seismic anisotropy of Tonga slab. *Nature* **455**, 657–660 (2008).
- Ganguly, J., Cheng, W. & Chakraborty, S. Cation diffusion in aluminosilicate garnets: Experimental determination in pyrope–almandine diffusion couples. *Contrib. Mineral. Petrol.* **131**, 171–180 (1998).
- Gasparik, T. *Phase Diagrams for Geoscientists: An Atlas of the Earth's Interior* (Springer, 2003).

Acknowledgements

Funding of this project is provided by the European Commission through the Marie Curie Research Training Network ‘c2c’ (Contract No. MRTN-CT-2,006-035957) and the Leibniz programme of the Deutsche Forschungsgemeinschaft (LA 830/14-1).

Author contributions

All authors contributed in writing the paper. F.L. and W.L.v.M. conceived the idea for the experiments. F.L. supervised the project. D.J.F. and D.C.R. provided further advice for developing the experimental strategy. W.L.v.M. performed the experiments, conducted the TEM measurements and carried out the data reduction. Numerical modelling was performed by W.L.v.M.

Additional information

Supplementary information is available in the online version of the paper. Reprints and permissions information is available online at www.nature.com/reprints. Correspondence and requests for materials should be addressed to W.L.v.M.

Competing financial interests

The authors declare no competing financial interests.

1 **Stagnation of subducting slabs in the transition zone due to slow**
2 **diffusion in majoritic garnet**

3 **Authors:** W.L. van Mierlo, F. Langenhorst, D.J. Frost, D.C. Rubie
4
5
6

7 **Supplementary information: Methods**

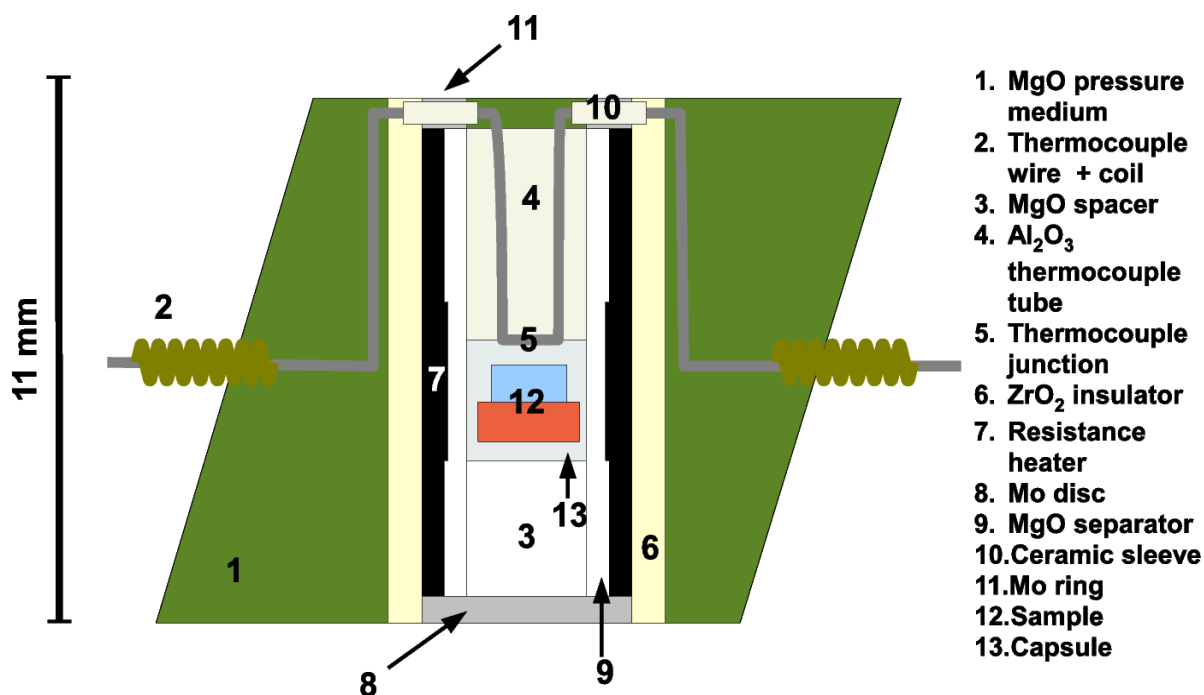
8 *Starting Materials and High-Pressure Experiments*

9 Diffusion experiments were conducted using the diffusion couple method, i.e. two cylinders
10 of garnet with their faces mirror polished were placed together in a capsule and then annealed
11 at high pressure. The garnet cylinders consisted of polished cylinders of polycrystalline
12 synthetic majoritic garnet (composition $\text{Py}_{55}\text{Mj}_{45}$) and natural pyrope garnet ($\text{Py}_{93}\text{Alm}_5\text{Gr}_2$)
13 single crystal from the Dora Maira Massif in Italy¹ to determine pyrope – majorite
14 interdiffusivity. The compositions of the starting materials are listed in Supplementary Table
15 1. Furthermore, FTIR spectra were measured to determine the water contents in garnets using
16 the calibration of Bell². The measurements reveal very low water contents, the highest
17 concentration of 58(6) ppm wt H_2O was determined for pyrope and showed no change during
18 the experiment. For majorite the water content was only determined after the experiment and
19 was about 37(4) ppm wt H_2O .

20 Since majoritic garnet is not commonly found in nature, it was synthesized using the multi-
21 anvil technique. First, reagent grade MgO , Al_2O_3 and SiO_2 oxide powders were ground and
22 mixed under ethanol. The resulting powders were then fused in a furnace at 1650 °C and
23 quenched to a glass. To thoroughly homogenize the starting material, the glass was crushed,
24 ground and fused a second time. The final glass was crushed to a powder that was then loaded
25 into a Pt capsule (inner diameter 0.8 mm, outer diameter 1.2 mm, length 2.2 mm) for
26 synthesizing majoritic garnet. Just before the synthesis experiments, the loaded capsule was
27 heated for 5 minutes at 1000 °C to dry the powder, after which it was sealed mechanically.
28 Majoritic garnet was then synthesized in a multi-anvil apparatus using a 10/5 assembly

29 (numbers denote octahedron edge length and WC cube truncation edge length in mm,
30 respectively) at 1800 °C and 16 GPa for 8 hours. After recovery the platinum capsule was cut
31 into discs of 0.5 mm thickness and one side was polished, where the final polishing was
32 performed using a 0.25 µm diamond polishing paste. The final surface topography was
33 measured using a confocal microscope and for the single crystal pyrope was determined to be
34 ~ 3 nm over a lateral length of ~ 25 µm and for the polycrystalline majoritic garnet cylinders
35 ~ 20 nm over a lateral length of ~ 25 µm. The average grain size of the synthetic majoritic
36 garnet was 5 – 10 µm.

37 Before the diffusion experiments, the samples were dried in a vacuum oven at 175 °C for 24
38 hours, after which the capsules were mechanically sealed as fast as possible in a bench vice.
39 The diffusion experiments were carried out in a 1000 ton multi-anvil apparatus at the
40 Bayerisches Geoinstitut. Each diffusion couple was contained within a platinum capsule. A W
41 3% Re - W 25% Re thermocouple was used to measure the temperature. To prevent the
42 thermocouple from reacting with the capsule, it was separated from the capsule with a 25 µm
43 thick Re disk. After the pressure cell was loaded in the multi-anvil apparatus the sample was
44 compressed to the desired pressure and then the temperature was increased at a rate of 100 °C
45 / minute, with the final 200 °C being achieved in one minute. Quenching was performed by
46 cutting the electrical power, which results in the sample temperature decreasing to 100 °C in
47 ~10 seconds.



48

49 *Supplementary Figure 1: Sketch of the pressure cell used in the diffusion anneals.*

50

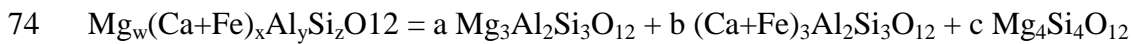
51 *Analytical methods*

52 After recovery of the sample, the capsule was cut perpendicular to the interface between the
 53 two halves of the diffusion couple and was prepared as a 30 µm thick thin section. These thin
 54 sections were subsequently analysed by a JEOL JXA-8200 electron microprobe to determine
 55 the length of the diffusion profiles. Since in all cases the diffusion profiles were too short to
 56 be measured by electron microprobe, the samples were further prepared for TEM by ion
 57 milling with a conventional Gatan DUOMILL and a FEI Quanta 3D FEG dual beam device
 58 (FIB/SEM). TEM foils were analyzed in a Philips CM20 FEG TEM operating at 200 kV and
 59 being equipped with an ThermoNoran EDS system. To ensure that the beam direction, and
 60 thus excitation volume for EDS analysis, was perpendicular to the diffusion gradient, the
 61 TEM foil was oriented in such a way that one of rotation axes of the specimen holder was
 62 parallel to the diffusion interface and the other one was perpendicular to it.

63 Diffusion profiles were measured in STEM mode with a slightly-defocused beam to avoid

64 beam damage. The scanning pattern size of a single analysis is ~ 40 nm. In the case that beam

65 damage was still observed, a time series was measured to quantify the beam damage and
 66 correct for it. Analyses were quantified using a method similar to that proposed in Van
 67 Cappellen and Doukhan³.
 68 The garnet component mole fractions are calculated from the elemental compositions using a
 69 least squares technique. Since Fe has a strong prevalence for the dodecahedral site⁴ it is
 70 assumed that the Fe-majorite component (FeSiO₃) is negligible in the majorite garnet. For the
 71 pyrope – majorite garnet analyses, the grossular and almandine components have been taken
 72 together as one virtual component (Ca+Fe)₃Al₂Si₃O₁₂, leading to the following components to
 73 be calculated from the elemental compositions:



75 for which the following matrix equation can be written and solved:

76

77
$$\begin{bmatrix} 3 & 0 & 4 \\ 0 & 3 & 0 \\ 2 & 2 & 0 \\ 3 & 3 & 4 \end{bmatrix} \cdot \begin{bmatrix} a \\ b \\ c \end{bmatrix} = \begin{bmatrix} w \\ x \\ y \\ z \end{bmatrix} \quad (1)$$

$A \cdot c_{comp} = c_{element}$

78 The errors on the component compositions are calculated using the following formula, which
 79 can be obtained from the propagation of errors:

80

81
$$M^{comp} = A^+ \cdot M^{element} \cdot (A^+)^T \quad (2)$$

82 where $M^{element}$ is the covariance matrix of the elemental concentrations and where the
 83 diagonal elements (variances) are the squared errors of the elemental concentrations, which
 84 were estimated from the relative errors of the counting statistics. The off-diagonal elements
 85 were set to zero (zero covariance between elements). A^+ denotes the Moore – Penrose
 86 pseudoinverse of A, and the superscript T denotes the transpose.

87

88 *Numerical modeling of diffusion profiles*

89 Because the shape of the diffusion profiles did not give any indications for a composition
90 dependent diffusion coefficient, the diffusion profiles have been modeled using the following
91 equation:

92

93
$$\frac{\partial C_i}{\partial t} = D_i \frac{\partial^2 C_i}{\partial x^2} \quad (3)$$

94 where C_i , t , x , and D_i are the concentration of component i , time, spatial coordinate and the
95 diffusion coefficient for component i , respectively. D_i has been assumed to be composition
96 independent in this study, because using compositionally-dependent diffusion coefficients did
97 not significantly improve the fits. The modeling and fitting of diffusion profiles was done by
98 two programs (mcdiff and mcfitter), which solve equation (3) using a finite difference
99 approach. The Levenberg-Marquardt algorithm has been employed for the fitting of
100 calculated diffusion profiles to the measured ones. The confidence intervals of the diffusion
101 coefficients have been determined using the bootstrap method with resampling of residuals⁵.
102 In addition to determining the diffusion coefficients, this study includes also the determination
103 of temperature and pressure dependence of the diffusivity of the majorite component in
104 garnet. The dependence on these variables has been expressed by an Arrhenius relation:

105

106
$$\ln D_i^0(T) = \ln D_i^0 - \frac{\Delta H}{RT} \quad (4)$$

107 where the activation enthalpy is expressed as $\Delta H = \Delta E + P\Delta V$. Here P , T , R , ΔE , and ΔV are
108 pressure, temperature, the gas constant, and the activation energy and activation volume for
109 diffusion of the majorite component in garnet, respectively. The values and error bounds of
110 activation enthalpy, activation energy, activation volume and the pre-exponential factors were

111 determined using the weighted least squares method (weights inverse proportional to the
112 variances), though using the normal least squares method did not give significant different
113 results.

114

115

116 *Modeling of pyroxene dissolution in garnet*

117 To model diffusion in a grain together with diffusion-controlled growth a finite difference
118 model was used. The basic equation that governs diffusion in a spherically symmetric
119 geometry assuming a constant diffusion coefficient D is given by⁶:

120

$$121 \quad \frac{\partial C}{\partial t} = D \left(\frac{2}{r} \frac{\partial C}{\partial r} + \frac{\partial^2 C}{\partial r^2} \right) \quad (5)$$

122 where C is the concentration, r the radial distance from the centre, t time and D the diffusion
123 coefficient,. Equation 5 has been discretized using a fully implicit scheme⁷:

124

$$125 \quad C_i^k = -\alpha \left(\frac{1}{\Delta r} + \frac{1}{r_i} \right) C_{i+1}^{k+1} + \left(1 + \frac{2\alpha}{\Delta r} \right) C_i^{k+1} - \alpha \left(\frac{1}{\Delta r} - \frac{1}{r_i} \right) C_{i-1}^{k+1} \quad (6)$$

with $\alpha = \frac{D\Delta t}{\Delta r}$

126

127 where k is the time index, i the spatial index, Δr the distance between two nodes, and Δt the
128 time step for temporal discretization. Equation 6 leads to a system of linear equations that
129 may be represented in a matrix form involving a tridiagonal matrix that can be solved using
130 standard methods included in the LAPACK software⁸. The code has been tested against a
131 steady state analytical solution for a hollow sphere.

132 Because the solubility of aluminium in pyroxene at the conditions of the transition zone is
133 very low⁹ and thus there cannot be a direct transformation of pyroxene into garnet, dissolution
134 of pyroxene in garnet will not occur by a simple exchange mechanism. Therefore the garnet
135 grain needs to grow during dissolution of pyroxene into garnet. Grain growth (or shrinkage)
136 was modeled by dividing the domain into three parts; the internal part, the boundary and the
137 external part. The internal part corresponds to the grain and for this part equation 6 is solved
138 for every time step. The boundary has a constant concentration, that corresponds to the
139 equilibrium concentration of the grain in contact with the external phase, and its position
140 determines the size of the external and internal part. The external part is a volume reservoir to
141 allow for grain growth or shrinkage and has a constant concentration, not necessarily equal to
142 the boundary concentration. If the boundary concentration is different from the concentration
143 of the internal part, material will flow in or out of the grain. The total flux of material that has
144 diffused into or out of the grain is determined after every time step by integration of the
145 concentration profile over the complete grain, taking into account the proper geometry. The
146 boundary position is then updated for the next time step based on the total mass of material
147 that has moved in/out of the grain (M_{int}) and the concentration or density of material in the
148 external part:

$$149 \quad \Delta V_{grain} = \frac{M_{int} - M_0}{C_{ext}} \quad (7)$$

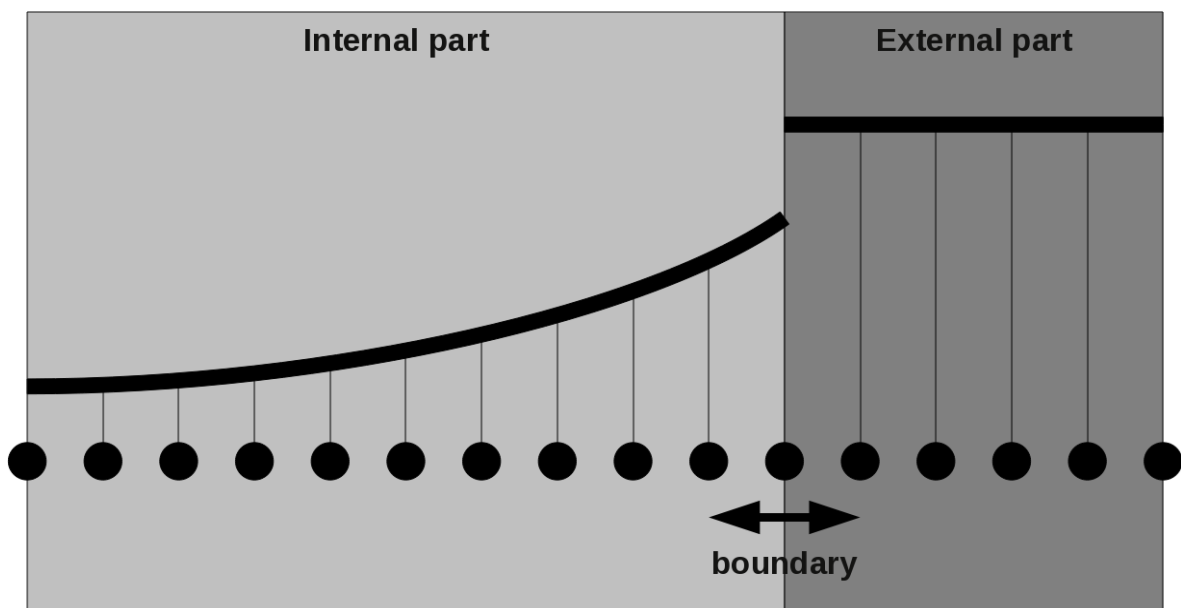
150 M_0 is the starting concentration of material in the grain and C_{ext} the concentration in the
151 external part. ΔV_{grain} is the change in volume of the grain. In the case of grain growth, the
152 composition of the new nodal points in the internal part is set to the boundary composition
153 (Supplementary fig. 2).

154 The growth of the grain can be stopped after a certain amount of material has diffused into the
155 grain. The boundary position is kept constant after this point has reached. To stop material

156 from flowing in or out of the grain, the boundary flux is forced to be zero using a Neumann
157 boundary condition:

158
$$C_b^{k+1} - C_{b-1}^{k+1} = 0 \tag{8}$$

159 where b is the boundary node. In the case that the internal part contains the first node, also a
160 Neumann type boundary condition was used for the first node. In this study diffusion of the
161 majorite component into the garnet grain has been stopped at the point where the mean
162 concentration is $\text{Py}_{60}\text{Mj}_{40}$, i.e. after complete homogenization the grain would have this
163 composition. This garnet equilibrium composition corresponds to experiments conducted on
164 refractory MORB material after partial melting and transformation to an eclogite assemblage,
165 representative of the subducted oceanic crust⁹.



166
167 *Supplementary Figure 2: Sketch of the discretization model used in the numerical model for*
168 *the calculation of the dissolution of pyroxene into garnet.*

169

170 **References**

- 171 1. Schertl, H.-P., Schreyer, W. & Chopin, C. The pyrope-coesite rocks and their country rocks
172 at Parigi, Dora Maira Massif, Western Alps: detailed petrography, mineral chemistry and
173 PT-path. *Contrib Mineral Petrol* **108**, 1–21 (1991).
- 174 2. Bell, D. R., Ihinger, P. D. & Rossman, G. R. Quantitative analysis of trace OH in garnet
175 and pyroxenes. *Am Mineral* **80**, 465–474 (1995).
- 176 3. Van Cappellen, E. & Doukhan, J. C. Quantitative transmission X-ray microanalysis of
177 ionic compounds. *Ultramicroscopy* **53**, 343–349 (1994).
- 178 4. O'Neill, H. S. C. *et al.* Mössbauer spectroscopy of mantle transition zone phases and
179 determination of minimum Fe³⁺ content. *Am Mineral* **78**, 456–461 (1993).
- 180 5. Efron, B. & Tibshirani, R. J. *An Introduction to the Bootstrap*. (Chapman and Hall/CRC,
181 1994).
- 182 6. Crank, J. *The Mathematics of Diffusion*. (Oxford University Press, USA, 1980).
- 183 7. Fletcher, C. A. J. *Computational Techniques for Fluid Dynamics 1*. **1**, (Springer, 2005).
- 184 8. Anderson, E. *et al.* *LAPACK Users' Guide*. (Society for Industrial and Applied
185 Mathematics, 1999).
- 186 9. Irifune, T., Sekine, T., Ringwood, A. E. & Hibberson, W. O. The eclogite-garnetite
187 transformation at high pressure and some geophysical implications. *Earth Planet Sci Lett*
188 **77**, 245–256 (1986).
- 189
190

191 **Supplementary tables**

192 *Supplementary Table 1:* Electron microprobe analyses of the starting materials in wt. % and
 193 cations per 12 oxygens.

Oxide	Dora Maira pyrope	Majorite garnet
MgO	27.49	34.37
SiO ₂	44.13	51.57
CaO	0.61	0.00
MnO	0.05	0.00
FeO	2.51	0.02
Al ₂ O ₃	24.84	12.59
TiO ₂	0.02	0.00
Total wt. %	99.65	98.55
Mg ²⁺	2.79	3.48
Ca ²⁺	0.05	0.00
Fe ²⁺	0.14	0.00
Fe ³⁺	0.00	0.00
Al ³⁺	2.00	1.01
Ti ⁴⁺	0.00	0.00
Si ⁴⁺	3.01	3.50

194

1 Stagnation of subducting slabs in the transition zone due to slow 2 diffusion in majoritic garnet

3 Authors: W.L. van Mierlo, F. Langenhorst, D.J. Frost, D.C. Rubie
4

5 Supplementary Notes

6 *Note on the effective diffusivity of a polycrystalline aggregate*

7 The effective diffusion coefficient can be expressed as $D_{\text{eff}} = f D_{\text{gb}} + (1 - f)D_{\text{vol}}$, where f is the
8 grain boundary volume fraction and D_{gb} the grain boundary diffusivity¹. Assuming that the
9 grain boundary width is 1 nm, diffusion distance enhancement factors range from 1 to 50 for a
10 100 μm grain for grain boundary diffusion rates from $10^3 \times D_{\text{vol}}$ to $10^8 \times D_{\text{vol}}$. For 1 mm
11 grains the enhancement factors range from 1 to 17.

13 *Note on the migration of the interfacial grain boundary in the diffusion couples*

14 All majoritic garnet – pyrope garnet diffusion couples showed that after the diffusion anneals
15 the grain boundary that formed the interface between both diffusion couples migrated into the
16 majoritic garnet half of the diffusion couple. We believe that this is caused by a process
17 similar to Oswald ripening, i.e. the smaller grains (majoritic aggregate) are consumed by the
18 larger grains (pyrope crystal) and thereby reducing the total surface energy. There is virtually
19 no strain at the diffusion interface after grain boundary migration occurred, because of great
20 similarity between the lattice parameters of majoritic garnet and pyrope². Therefore from the
21 point of view of grain boundary migration the whole diffusion couples acted as a single phase
22 aggregate. The orientation of the interface was determined in the experiments by measuring
23 several diffusion profiles and in this way the position of the interface at several locations was
24 determined. We don't believe that this process influenced the determined diffusion
25 coefficients, because the width of dry grain boundaries is not more than a few nanometer at
26 most and the region of influence is confined to this range. If it would have influenced the

27 experiment at all, it would have brought it closer to a true bulk diffusivity measurement,
28 removing the influence of nearby grain boundaries.

29

30 **References**

- 31 1. Hart, E. W. On the role of dislocations in bulk diffusion. *Acta Metall* **5**, 597 (1957).
32 2. Heinemann, S., Sharp, T. G., Seifert, F. & Rubie, D. C. The cubic-tetragonal phase
33 transition in the system majorite ($\text{Mg}_4\text{Si}_4\text{O}_{12}$) – pyrope ($\text{Mg}_3\text{Al}_2\text{Si}_3\text{O}_{12}$), and garnet
34 symmetry in the Earth's transition zone. *Phys Chem Miner* **24**, 206–221 (1997).
35

on the circumpolar westerlies, rather than stratospheric ozone depletion.

Steig and colleagues⁹ find a more subtle change hidden in the oxygen isotopic composition of ice cores spanning West Antarctica. The oxygen isotope signature of ice is typically interpreted as a proxy for temperature. However, it also responds to wider circulation anomalies that have influenced the region, including changes in sea ice and wind-driven ocean changes. Steig *et al.* interpreted the isotope values in terms of these broader trends. They used an ice core from the West Antarctic Ice Sheet Divide that spanned 2,000 years, in conjunction with an array of shorter cores, to document unusually high oxygen isotope ratios in the 1990s. Comparable events occurred in just 1% of the time series studied. The trend in oxygen isotopes over the past 50 years at the divide is also unusual, with comparable trends present in just 2% of the records.

Building on previous work that identified tropical influences on West Antarctic climate, they link the isotopic anomalies to changes in atmospheric convection over the tropical Pacific Ocean, propagated to the high latitudes through atmospheric waves. An isotope-equipped climate model, fed with tropical Pacific sea surface temperatures, reproduces the prominent isotope anomaly in the 1990s

that is recorded in the West Antarctic ice cores. Interestingly, the authors note that the Pacific variability associated with this 1990s anomaly was not outside the natural range of variability observed over past centuries.

Although the tropical drivers of the West Antarctic isotopic anomalies may not be unprecedented, the very existence of a link adds to concerns about future change in the region. A strong influence of tropical processes on the climate of West Antarctica adds an extra source of uncertainty in estimates of the manifestation of greenhouse-gas-induced climate change. Steig and colleagues also suggest that the decadal-scale variability in the tropics has masked the local Antarctic response to anthropogenic forcing.

These studies remind us that we should not expect Antarctic climate change to be uniform in time or space. The climate response is mediated by multiple processes, each having varied seasonal and geographical expressions, linked by hemispheric and global scale connections, and subject to decadal-scale variability that can confound detection of the forced signal. Improvements in capturing these processes in models and testing with improved data, both observational and palaeoclimatic, are the keys to predicting the patterns and rates of change.

Individually, the ice core records presented by Abram *et al.*⁸ and Steig *et al.*⁹ add to the evidence that changes currently seen in Antarctica are unusual relative to the past 2,000 years. Taken together, alongside other indicators of change, the message is becoming clearer: Antarctica is very likely to be showing a response to the warming climate of the planet. □

Tas van Ommen is at the Australian Antarctic Division, Channel Highway, Kingston, 7050 Tasmania, Australia, and at the Antarctic Climate and Ecosystems Cooperative Research Centre, University of Tasmania, Sandy Bay 7050, Tasmania, Australia.
e-mail: tas.van.ommen@aad.gov.au

References

1. Shepherd, A. *et al.* *Science* **338**, 1183–1189 (2012).
2. Scambos, T. A., Hulbe, C. & Fahnestock, M. in *Antarctic Peninsula Climate Variability: Historical and Palaeoenvironmental Perspectives*, Antarctic Research Series Vol. 79 (eds Domack, E. *et al.*) 79–92 (American Geophysical Union, 2004).
3. Stammerjohn, S., Massom, R., Rind, D. & Martinson, D. *Geophys. Res. Lett.* **39**, L06501 (2012).
4. Steig, E. J. *et al.* *Nature* **457**, 459–462 (2009).
5. Bromwich, D. H. *et al.* *Nature Geosci.* **6**, 139–145 (2013).
6. Muto, A., Scambos, T. A., Steffen, K., Slater, A. G. & Clow, G. D. *Geophys. Res. Lett.* **38**, L15502 (2011).
7. Screen, J. A. & Simmonds, I. *J. Geophys. Res.* **117**, D16108 (2012).
8. Abram, N. J. *et al.* *Nature Geosci.* **6**, 404–411 (2013).
9. Steig, E. J. *et al.* *Nature Geosci.* **6**, 372–375 (2013).
10. Mulvaney, R. *et al.* *Nature* **489**, 141–144 (2012).
11. Thompson, D. W. J. *et al.* *Nature Geosci.* **4**, 741–749 (2011).
12. Trusel, L. D., Frey, K. E. & Das, S. B. *J. Geophys. Res.* **117**, F02023 (2012).

MINERALOGY

Garnet goes hungry

Sinking slabs of oceanic lithosphere often stagnate in Earth's mantle. Experiments show that common slab minerals transform to their high-pressure, high-density counterparts at very slow rates, thus keeping the slabs buoyant and impeding subduction.

Craig R. Bina

Students in the petrology lab learn quickly that the mineral garnet — an abundant component of the Earth's mantle — 'eats' everything. Indeed, this mineral's complex crystalline structure can accommodate a bewildering variety of cations. Writing in *Nature Geoscience*, van Mierlo *et al.*¹ use high-pressure and high-temperature experiments to show that garnet dines rather slowly, at least under conditions prevailing in subduction zones, with important implications for subduction dynamics and mantle chemistry.

Slabs of oceanic lithosphere contain abundant amounts of the minerals garnet

and pyroxene. As the slabs sink into the mantle, the pyroxene is thought to dissolve into the denser garnet, where it forms a component known as majorite². The rate at which such dissolution occurs, however, is controlled by how fast majorite can diffuse through the garnet structure. High pressures within the mantle should cause the remaining components of the subducting oceanic slab — dominated by the mineral olivine — to also undergo phase transitions, thus increasing the slab's density as it sinks deeper into the Earth. Yet in seismic images of Earth's interior, the slabs often seem to stall near the base of the mantle transition zone, which is a region

located between 410 and 660 km depth. This stalled subduction may be linked to these complex mineral transformations that occur within the slab.

Our understanding of how pyroxene in an oceanic slab dissolves into garnet is based on laboratory experiments. In an attempt to simulate these transformations, which occur over long geological timescales and at hundreds of kilometres depth in the mantle, the samples are usually ground into fine powders that are squeezed and heated. Yet, in real subduction zones, grain sizes within subducting slabs are large and the temperatures in the slab are low compared with the warm surrounding mantle.

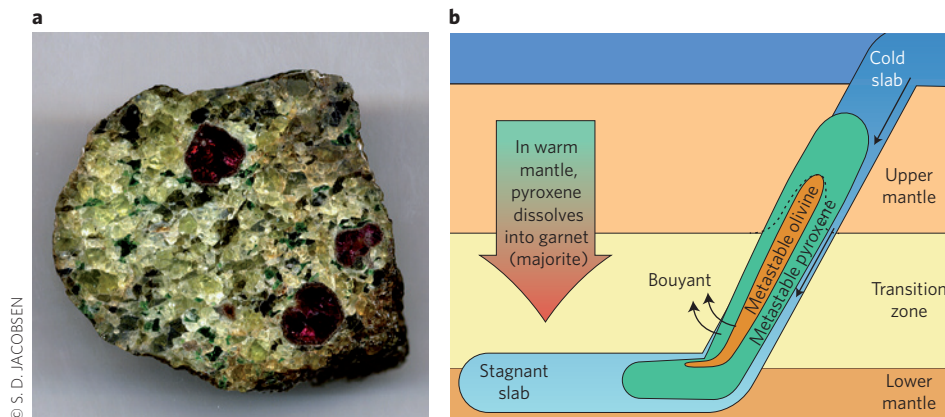


Figure 1 | Subduction of oceanic lithosphere in the mantle transition zone. **a**, Slabs of oceanic lithosphere contain a variety of minerals including olivine (pale green), pyroxene (dark green) and garnet (red). **b**, As the slab subducts into the mantle, it encounters higher temperatures and pressures that cause the minerals to undergo phase transformations. The common slab mineral pyroxene dissolves into garnet, forming the component majorite within the garnet. Similarly, the olivine transforms to denser phases. Van Mierlo and colleagues¹ use laboratory experiments to show that majorite is one of the slowest diffusing components of the mantle. Further dissolution of pyroxene is therefore inhibited and the pyroxene persists in a metastable, buoyant state that can potentially slow and deflect subduction.

A first step towards improved understanding of these transitions was to carry out experiments and modelling to explore reaction kinetics at the relatively low slab temperatures. The results suggested that, although olivine and pyroxene were expected to become unstable under the high-pressure conditions of Earth's mantle, they might instead remain in a metastable (and thus buoyant) state^{3–5}. Pyroxene was kinetically inhibited from dissolving into garnet⁶, but the relevant diffusion rates remained unknown.

Now van Mierlo *et al.*¹ have taken the next step. They use laboratory experiments to measure precisely (at the micrometre scale) the rate at which the majorite component — formed by the dissolution of pyroxene into garnet — diffuses through the garnet structure, over a range of high pressures and temperatures. The results are extrapolated to the conditions of the mantle transition zone, and they are striking. It turns out that garnet is a very slow eater. Even at high temperatures and pressures of 1,800 °C and 15 GPa — warmer than the corresponding depth in the mantle transition zone — the rate of majorite diffusion is extremely low, with a diffusion coefficient below $10^{-18} \text{ m}^2 \text{ s}^{-1}$. This rate of diffusion is comparable to the diffusion of magnesium in garnet at much lower temperatures and pressures, below 1,000 °C at 1 GPa (ref. 7). Majorite therefore seems to be one of the most slowly diffusing components in the mantle.

The slow diffusion of majorite has two important implications for mantle chemistry and geodynamics. First, majorite components formed in the mantle may persist over very long timescales. Van Mierlo and colleagues extrapolate the diffusion data to realistic grain sizes for oceanic slabs (on the order of millimetres) and show that majorite-bearing heterogeneities formed in the mantle transition zone would be homogenized at length-scales of, at most, tens of metres over timescales comparable to the age of the planet. Yet subducted slabs are typically thousands of metres thick, meaning that the majorite components will not fully homogenize and may remain as chemical anomalies in the transition zone for billions of years. This finding supports suggestions that the mantle transition zone may be a mechanical mixture of different components, rather than a homogenized unit⁸.

Second, there is the prospect of metastable pyroxene persisting to depths at which it should have been devoured by garnet. Entry of pyroxene into the garnet structure as majorite is controlled by the rate of majorite diffusion. Thus, the slow diffusion of majorite prevents pyroxene being dissolved into the garnet, and the garnet goes hungry. Pyroxene is less dense than garnet, and its persistence will impart positive buoyancy to the slab, thereby impeding subduction (Fig. 1). Similar buoyancy perturbations have been posited for other slab minerals, such as metastable olivine, at temperatures below about 700 °C

in the coldest core of the slab⁴. However, the new diffusion data imply that pyroxene can remain metastable and buoyant to temperatures as high as 1,400 °C, extending the potential for metastability over a much larger area of the slab and thereby amplifying the buoyancy effect.

The slow diffusion of majorite can therefore help explain the stagnation of subducting slabs in the mantle transition zone. The metastable pyroxene may remain undigested for some time, and the positive buoyancy would then generate slower slab descent rates and cause the wholesale flexure of the slab into a sub-horizontal stagnant posture in the transition zone. Such slab stagnation may persist until thermal assimilation warms the slab sufficiently to allow consumption or further reaction (perhaps to metastable akimotoite) of the buoyant metastable material.

The experiments illuminate the metastability of magnesium-rich pyroxene. However, complex natural pyroxenes may be more reactive than the magnesium-rich variety⁹. The behaviour of multi-component mineral assemblages with, for example, differing iron or hydrogen concentrations have yet to be fully investigated. Buoyancy relations are further complicated by the fact that, although metastable pyroxene may persist over a larger extent of the slab than metastable olivine, the latter is more buoyant than the former.

Van Mierlo *et al.*¹ demonstrate that garnet dines rather slowly, at least under conditions prevailing in subduction zones. Slow diffusion of majorite can inhibit the dissolution of pyroxene into garnet in subducting slabs, giving the slabs added buoyancy and causing them to stagnate in their descent through the mantle. Those investigating the chemistry, seismology and geodynamics of deep subduction will need to reflect on the dining habits of garnet. □

Craig R. Bina is in the Department of Earth and Planetary Sciences, Northwestern University, Evanston, Illinois 60208-3130, USA.
e-mail: craig@earth.northwestern.edu

References

1. Van Mierlo, W. L., Langenhorst, F., Frost, D. J. & Rubie, D. C. *Nature Geosci.* **6**, 400–403 (2013).
2. Akaogi, M. & Akimoto, S.-i. *Phys. Earth Planet. Inter.* **15**, 90–106 (1977).
3. Sung, C. M. & Burns, R. G. *Tectonophysics* **31**, 1–32 (1976).
4. Rubie, D. C. & Ross, C. R. *Phys. Earth Planet. Inter.* **86**, 223–243 (1994).
5. Hogrefe, A., Rubie, D. C., Sharp, T. G. & Seifert, F. *Nature* **372**, 351–353 (1994).
6. Nishi, M., Kubo, T. & Kato, T. *J. Miner. Petrol. Sci.* **104**, 192–198 (2009).
7. Carlson, W. D. *Am. Mineral.* **91**, 1–11 (2006).
8. Xu, W., Lithgow-Bertelloni, C., Stixrude, L. & Ritsema, J. *Earth Planet. Sci. Lett.* **275**, 70–79 (2008).
9. Lockridge, J. S., Sharp, T. G. & Leinenweber, K. D. AGU Fall Meeting abstr. DI24A-2369 (American Geophysical Union, 2012).